Physica Medica 64 (2019) 245–251

Contents lists available at ScienceDirect

Physica Medica

journal homepage: www.elsevier.com/locate/ejmp

Original paper

Internal dosimetry for TARE therapies by means of GAMOS Monte Carlo simulations

Lucrezia Auditore[a,b], Ernesto Amato[a,b,*], Antonio Italiano[b,c], Pedro Arce[d], Alfredo Campennì[a,e], Sergio Baldari[a,e]

[a] Section of Radiological Sciences, Department of Biomedical and Dental Sciences and Morphofunctional Imaging, University of Messina, Italy
[b] Istituto Nazionale di Fisica Nucleare, Sezione di Catania, Italy
[c] MIFT Department, University of Messina, Italy
[d] Medical Applications Unit, Centro de Investigaciones Energéticas, MedioAmbientales y Tecnológicas (CIEMAT), Madrid, Spain
[e] Nuclear Medicine Unit, University Hospital "G. Martino", Messina, Italy

ARTICLE INFO

Keywords:
Internal dosimetry
TARE
Monte Carlo
GAMOS
GEANT4

ABSTRACT

Three-dimensional internal dosimetry is increasingly used in planning Trans-Arterial Radio-Embolization (TARE) of HepatoCellular Carcinoma (HCC). Among the existing calculation approaches, Monte Carlo (MC) simulation is the gold standard. Aim of this work was to carry out a retrospective study of clinical cases of TARE to compare the performances of different computation approaches. We developed a procedure exploiting GAMOS (GEANT4-based Architecture for Medicine-Oriented Simulations) MC. Three dimensional absorbed dose maps, dose profiles and Dose Volume Histograms (DVHs) were produced for liver through MC simulations and convolution method implemented in STRATOS software. We compared the average absorbed doses with results of Medical International Radiation Dose (MIRD) approach.

For most patients, a reasonable agreement was found, with relative differences in mean doses within (−20.2%, +15.6%) for MIRD *vs*. MC and (−12.1%, +7.6%) for STRATOS *vs*. MC. Discrepancies can mainly be related to the gamma-rays contribution, more precisely taken into account in MC.

For one patient we evaluated through MC simulation a lung dose of about 2 Gy coming from pulmonary shunt (96%) and from irradiation from liver (4%), with values up to 4.5 Gy near liver-lung interface.

3D dosimetry for TARE treatments can be satisfactorily carried out with convolution methods as long as VOIs of regular shape are considered. MC simulations are more appropriate for VOIs where the contribution from gamma-rays has to be carefully taken into account. The absorbed dose distribution in presence of relevant tissue inhomogeneities can be assessed accurately by means of MC simulations only.

1. Introduction

Internal dosimetry plays a growing role in planning and monitoring nuclear medicine therapies [1]. Thanks to more and more precise methodological approaches, also relying on higher quality imaging data, the uncertainties in results are shrinking, leading to a better precision in dosimetric estimates and, finally, to a closer relationship between dosimetric indicators, biological effects, and clinical outcomes [2–5].

In order to estimate the uneven distribution of radiation absorbed doses in organs and tissues where the radiopharmaceutical uptake is not uniform, three dimensional internal dosimetry approaches, based either on the convolution of voxel S factors or absorbed dose point-kernels, were developed [6–9]. Both methods, however, can suffer from two limitations potentially leading to some degree of inaccuracy. First, usually they assume an uniform (often unitary) material density, neglecting the remarkable differences between human tissues, such as inflated lungs, soft tissue and bone [10,11]. Nevertheless, some Authors developed convolution methods in heterogeneous media [12]. Secondly, due to computation requirements, the convolution is generally truncated to a limited range around the calculation point, so that the contribution of deep-penetrating radiations (gamma-rays) is neglected above a certain distance; in the voxel S factors approach is usually equal to five voxels [13].

In order to overcome these limitations, some researchers and groups set up Monte Carlo (MC) simulation tools able to input transmission and

* Corresponding author at: Section of Radiological Sciences, Department of Biomedical and Dental Sciences and Morphofunctional Imaging, University of Messina, Italy.
E-mail address: eamato@unime.it (E. Amato).

https://doi.org/10.1016/j.ejmp.2019.07.024
Received 7 May 2019; Received in revised form 26 July 2019; Accepted 27 July 2019
Available online 02 August 2019

emission tomography data to get information about the tissue density and radionuclide source distributions within patient's body [14–22].

Among nuclear medicine therapies, Trans-Arterial Radio-Embolization (TARE) of HepatoCellular Carcinoma (HCC) is a therapy increasingly used to treat patients with primary or secondary hepatic malignancies. To find a good compromise between therapy effectiveness and patient safety, high accuracy internal, patient-specific dosimetry is needed for planning the treatment.

In the present work, we carried out a retrospective study on clinical cases of TARE of HCC. For seven patients we set up a MC internal dosimetry procedure exploiting the user-friendly package GAMOS (GEANT4-based Architecture for Medicine-Oriented Simulations) in order to estimate the absorbed dose distribution in liver and surrounding organs. Particular attention was focused on lungs whose irradiation originates from ^{90}Y-microspheres delivered through pulmonary shunt and external irradiation from liver.

2. Materials and methods

We retrospectively performed a dosimetric study of seven clinical cases of TARE of HCC. For this type of treatment, a preliminary diagnostic procedure had been carried out to study the distribution of the ^{90}Y-labelled glass microspheres in liver and the potential shunt in lungs, by means of ^{99m}Tc macroaggregated albumin (Tc-MAA) administration and scintigraphic imaging.

In detail, patients potentially enrolled for TARE treatment of HCC undergo multi-phase abdominal contrast-enhanced CT, for lesion localization. Then the angio-scintigraphic procedure consists of ^{99m}Tc-MAA administration followed by a planar (antero-posterior) whole body imaging for lung shunt evaluation and by abdominal SPECT acquisition.

SPECT images were acquired using 120 projections (3 degrees angular step), each made of 128×128 pixels, energy window of 15%, and reconstructed through iterative OSEM algorithm into cubic voxels, 4.664 mm side. Philips BrightView Dual Head gamma camera equipped with low energy, general-purpose collimators was used for planar and SPECT acquisitions.

Since the MAA induces embolization (without hemodynamic consequence) and stop in the capillaries where they are delivered, the effective decay time of that particular radiopharmaceutical coincides with the physical decay time, as no biological clearance occurs.

In these conditions, the dose to the soft tissue target can be calculated as [23,24]:

$$D = 49.67 \cdot \frac{A_0}{m} \tag{1}$$

where the absorbed dose, D, is in Gy, the administered activity, A_0, in GBq and the target mass, m, in kg. Eq. (1) is based on the MIRD schema for radiopharmaceutical dosimetry [25], assuming a homogenous activity distribution and a complete, local energy deposition within the target. In the treatment planning phase, the activity to be administered was calculated by Eq. (1) to deliver a therapeutic dose of 120–140 Gy to the target lobe, depending on the clinical state.

Concerning the Monte Carlo dosimetry, we defined a procedure in GAMOS 5.2.0 [26], a user-friendly interface of the GEANT4 code [27–29].

GAMOS allows using CT images in DICOM format as input to define a geometrical, voxelized phantom reproducing patient morphology. To this aim, GAMOS converts CT DICOM images in a logical volume. Voxel-specific density is determined through a bi-linear relationship with Hounsfield Units (HU), then five intervals of density identify the different chemical compositions of materials (air: 0.0–0.1 gcm^{-3}; lung: 0.1–0.85 gcm^{-3}; adipose tissue: 0.85–0.94 gcm^{-3}; soft tissue: 0.94–1.2 gcm^{-3}; bone: $>$ 1.2 gcm^{-3}). The number of materials was properly chosen to take into account the main density inhomogeneities of the human body in the thoraco-abdominal districts.

The voxelized phantom was placed, in the GAMOS reference system, according to the position information included in the DICOM file header. This phantom includes Volumes Of Interest (VOIs) representing organs or lesions. We registered and segmented the SPECT-CT images using the IMALYTICS Research Workstation (Philips) [30]. The contouring was carried out by an experienced operator (the same for all the patients considered in this study). The defined VOIs were: Liver, Liver Perfused, Healthy Liver, Healthy Liver Perfused, and Lesion. Liver and Lesion were manually segmented on contrast-enhanced CT (arteriographic phase), while Liver Perfused was segmented on SPECT using a thresholding method. Healthy Liver was then obtained by logically subtracting Lesion from Liver, whereas Healthy Liver Perfused resulted by logically subtracting Lesion from Liver Perfused.

As a result of the segmentation, a DICOM *RTSTRUCT* file was produced and passed to GAMOS for the definition of the structures in the voxelized phantom.

Concerning the ^{90}Y distribution, the total number of radionuclide decays occurring in a voxel indexed by (*i,j,k*), i.e. the Time-Integrated Activity (TIA), can be evaluated as [31]:

$$\tilde{A}^{ijk} = A_0^{ijk}\,\tau \tag{2}$$

where A_0^{ijk} is the fraction of administered activity reaching the (*i,j,k*) voxel and τ is the physical decay time of the nuclide.

Due to the proportionality between activity and time-integrated activity maps, SPECT data where used to model the radionuclide distribution, using the generator class named GmGenerDistPositionInVoxelsFromFile.

Radiation emissions were simulated according to the *RadioactiveDecay* module of GEANT4 [32], whose models are based on the Evaluated Nuclear Structure Data File (ENSDF) [33,34].

Concerning the physics interaction models, we adopted the parameterizations of the electromagnetic interactions optimized for low energies, as implemented in the *GmEMExtendedPhysics* package [32] which by default uses the Livermore low energy electromagnetic physics model and enables the atomic de-excitation. In order to accurately sample the spatial distribution of energy deposition, we set a range cut of 50 μm, significantly shorter than the voxel dimension, corresponding to an energy cut of about 15 keV for electrons in soft tissue.

10^8 events per simulation were generated to achieve statistical uncertainties (2σ) associated to the presented results below 5%. No variance reduction method was used.

Many information was retrieved as output of MC simulations. Firstly, we evaluated average absorbed doses in the VOIs and compared the results with the ones estimated by Eq. (1).

Further, 3D absorbed dose maps were obtained scoring the energy deposition in the whole voxelized phantom and used to build absorbed dose profiles and absorbed Dose Volume Histograms (DVHs) in selected VOIs.

The same distributions were evaluated also by means of a convolution method implemented in the software STRATOS, available on IMALYTICS Research Workstation, and compared with the results of MC simulations.

Through a dedicated protocol for TARE, STRATOS computes TIA maps from SPECT and convolutes it with a pre-loaded matrix of voxel S-factors. The influence of such factors and of time-integration methods on dosimetric calculations was studied in a previous article, also for ^{90}Y therapies [35].

For one of the seven patients (patient #5), for which a whole body CT was available, we defined two additional VOIs, Right Lung and Left Lung, to perform MC dosimetry. This patient exhibited an attenuation corrected lung shunt fraction of 2%, supposed equally distributed between both lungs. MC simulations considered this activity as uniformly distributed within lung volumes; consequently, lung doses resulted from a contribution coming from internal uptake due to pulmonary shunt and from another contribution related to the external exposure from liver.

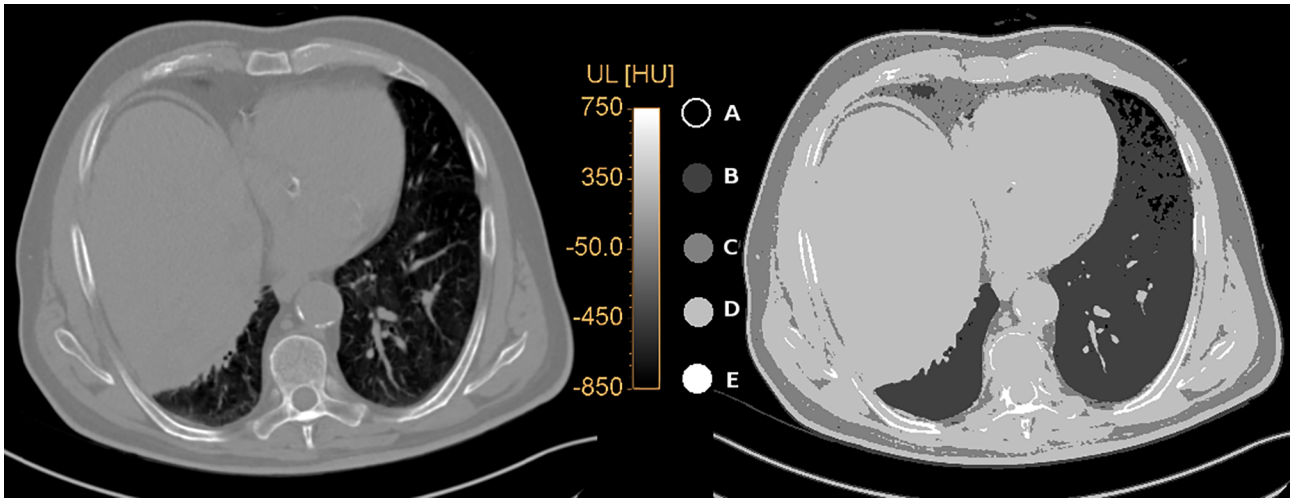

Fig. 1. (left) An axial CT slice of patient #2 showing upper liver and lungs; (right) the same slice of the GAMOS segmented phantom, where the grey levels represent the different materials: A: air; B: lung; C: adipose tissue; D: soft tissue; E: bone.

Table 1
Average radiation absorbed doses to the structures (VOIs). Comparison between MC, Eq. (1), and STRATOS results. Relative per cent differences are reported, taking MC results as reference.

	D_{MC} (Gy), ε_{MIRD} (%), $\varepsilon_{STRATOS}$ (%)				
	Liver	Liver Perfused	Lesion	Healthy Liver	Healthy Liver Perfused
1	**29.4**	**136.0**	**150.4**	**8.1**	**83.0**
	−3.1	2.1	0.1	−14.4	−9.3
	−2.8	−1.5	−1.6	−7.6	−6.4
2	**94.2**	**126.2**	**213.3**	**43.0**	**65.4**
	−2.0	4.3	1.5	−0.5	0.5
	3.3	4.6	5.5	6.9	7.6
3	**63.3**	**130.3**	**150.0**	**13.3**	**45.2**
	−2.0	0.5	0.4	−20.2	−3.8
	1.1	2.1	2.7	0.8	3.9
4	**44.6**	**140.1**	**222.4**	**17.4**	**83.2**
	−2.6	−3.9	6.1	−12.8	−3.5
	−0.8	2.8	3.9	−12.1	2.4
5	**52.8**	**133.0**	**137.0**	**10.1**	**76.0**
	−0.7	7.8	2.8	−16.5	−3.2
	2.5	5.2	5.8	1.8	1.2
6	**49.4**	**117.1**	**173.3**	**24.1**	**61.1**
	−5.4	11.3	−3.1	−9.7	−8.1
	−5.7	−3.5	−2.5	−8.5	−5.0
7	**56.3**	**105.3**	**229.2**	**44.3**	**81.4**
	3.9	15.6	6.8	−1.1	1.8
	−1.0	3.5	−0.5	1.9	3.5
ε_{MIRD} range (%)	(−5.4, +3.9)	(−3.9, +15.6)	(−3.1, +6.8)	(−20.2, −0.5)	(−9.3, +1.8)
$\varepsilon_{STRATOS}$ range (%)	(−5.7, +3.3)	(−3.5, +5.2)	(−2.5, +5.8)	(−12.1, +6.9)	(−6.4, +7.6)

3. Results

In Fig. 1, the result of GAMOS conversion of CT images to a segmented phantom is reported, clearly identifying five materials: air, lung, adipose tissue, soft tissue and bone.

Table 1 reports, for all patients, the average absorbed doses to the five liver structures and the relative per cent differences of doses from Eq. (1) and from STRATOS with respect to MC results, indicated as ε_{MIRD} and $\varepsilon_{STRATOS}$, respectively.

For most patients, a reasonable agreement between the three approaches was found; we estimated relative per cent differences within the ranges (−20.2%, +15.6%) for MIRD *vs.* MC and (−12.1%, +7.6%) for STRATOS *vs.* MC, respectively. The highest relative difference between absorbed doses estimated with Eq. (1) and MC simulations can be observed in Healthy Liver, where low values are registered.

In Table 2, masses of the considered liver structures are reported.

In Fig. 2(a), a SPECT-CT fusion image is shown with superimposed VOI contours. The corresponding dose maps are presented in panels (b) and (c), as obtained with MC simulations and STRATOS, respectively, for patient #2. In Fig. 3 the DVHs of the five structures are shown as

Table 2
Mass (g) of the structures (VOIs).

Patient #	Liver	Liver Perfused	Lesion	Healthy Liver	Healthy Liver Perfused
1	1266.3	239.5	189.1	1074.4	51.1
2	2200.6	1562.6	633.3	1581.2	929.8
3	1744.4	792.3	639.1	1119.9	153.2
4	2853.0	918.9	369.0	2479.4	542.5
5	2520.6	900.3	837.8	1706.2	76.3
6	2851.0	969.7	484.7	2466.2	485.0
7	2225.7	1040.6	169.7	2063.9	879.9

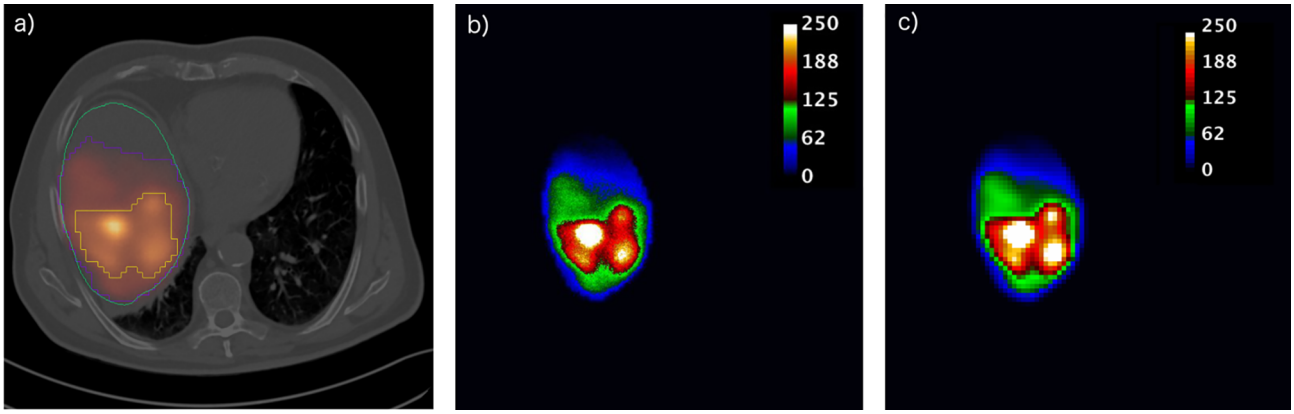

Fig. 2. (a) The fusion of CT and SPECT slices with VOI contours (green: Liver; blue: Liver Perfused; yellow: Lesion) for patient #2; the corresponding absorbed dose (Gy) map estimated with MC simulations (b) and STRATOS (c), respectively. (For interpretation of the references to colour in this figure legend, the reader is referred to the web version of this article.)

evaluated with these two approaches, for patient #6. DVHs of Healthy Liver Perfused for this patient exhibit the most relevant differences between the two calculation methods.

Dose maps and DVHs for the other patients are reported in Supplementary Materials.

For this patient, as a result of prescribing an average absorbed dose of 130 Gy to the Liver Perfused, which includes both lesions and the perfused part of the healthy liver, absorbed doses ranging from 20 to about 400 Gy were recorded in that volume. The whole Lesion receives at least 60–80 Gy, with about 30% of the volume absorbing more than 200 Gy. On the contrary, Healthy Liver exhibits a sharply decreasing DVH, with about 70% of its volume receiving less than 10 Gy and a few voxels with more than 100 Gy.

These outcomes confirm the treatment activity, decided on the basis of the comparison of average absorbed doses with the constraints derived by the clinical experience [26], i.e. $D_{\text{Healthy Liver}} < 60$ Gy, $80 < D_{\text{Liver Perf.}} < 150$ Gy, and expecting a higher efficacy in regions where $D_{\text{Lesion}} > 200$ Gy.

Finally, Fig. 4 shows the obtained dose map in the case of the only patient for which a whole body CT was available (patient #5); in particular, we report the dose map in one transversal slice next to the upper border of liver, where a maximum absorbed dose of about 4.5 Gy can be assessed. Table 3 reports the contributions to lung average absorbed dose coming from self (pulmonary shunt) and cross (liver → lung) irradiations. A mean absorbed dose to lungs of 2 Gy was estimated; about 4% of this dose is due to irradiation from perfused liver.

4. Discussion

For most patients, our results reveal a fair agreement between MC simulations and convolution calculations.

In particular, the relative per cent differences estimated for mean absorbed doses are within the range (−20.2%, +15.6%) for MIRD approach *vs.* MC simulations and within the range (−12.1%, +7.6%) for STRATOS convolution *vs.* MC simulations.

Concerning the comparison MIRD approach *vs.* MC simulations, for the VOI Liver an excellent agreement ($-5.4\% < \varepsilon_{\text{MIRD}} < 3.9\%$) was obtained for all patients and MIRD approach underestimates average absorbed doses for all the patients, except for patient #7. The most relevant differences can be observed in mean absorbed doses to the Healthy Liver, due to long-range irradiation from gamma-rays originating from the neighbouring perfused regions.

Analysing the comparison between STRATOS software and MC simulations in terms of mean absorbed doses, the agreement is very satisfying providing relative per-cent errors up to 6% for all the patients in Liver, Liver Perfused and Lesion.

Regarding the comparison between the DVHs obtained by the two calculation approaches, the hollow-shaped Healthy Liver Perfused exhibits a broader distribution of absorbed doses as shown in Fig. 3, attributable to gamma-rays contribution. Looking to the DVHs of the other cases provided in Supplementary Materials, the same behaviour is found also for patients #3 and #7, while the other four cases show a satisfactory agreement. These differences are attributable to the patient specific shape of Healthy Liver Perfused.

The discrepancies observed in DVHs for the Healthy Liver Perfused are not directly reflected to the mean absorbed dose. Indeed, as reported in Table 1, for patients #3-6-7, the relative differences between average absorbed doses estimated by MC simulations and STRATOS software are within ± 5% for Healthy Liver Perfused.

Our results compare well with those reported by other research groups. Hashkin et al. [22] carried out a similar comparison using Geant4 and a mathematical adult human phantom according to the MIRD Pamphlet 5 [36] considering three types of tissues (bone, soft tissue and lung). They reported relative differences up to 11% between the two methods, MC simulations and calculations performed with Eq. (1).

Also Petitguillaume at al. [21] reported a study based on a retrospective analysis of 10 clinical cases and using the OEDIPE software [37] for modelling the voxelized phantom and MCNPX code [38] for MC simulations. Relative differences between MC simulations and Eq. (1) of mean absorbed doses to tumour and non-tumour liver higher than 20% are reported when considering also the cross-fire effects.

As the same Authors point out, the most relevant contribution to the internal dosimetry of TARE treatments coming from such studies is the assessment of the absorbed dose distribution in lungs. We find that absorbed doses up to twice the average values can be reached near the base of right lung, i.e. in proximity to the liver/lung interface.

A further improvement of accuracy in dose evaluation might come from a scanner-specific CT calibration. This can be achieved by means of density-to-HU conversion function segmented by a stoichiometric method such as the one described in [39].

However, it is to be explicitly pointed out that the limited spatial resolution of SPECT scanners, affected both by intrinsic limitations in gamma camera resolution and by reconstruction algorithms and filters, leads to a blurred 3D estimation of TIA distribution. Such blurring implies a spill-out of counts from intensely uptaking regions and a reversed effect of spill-in through colder areas, leading to partial volume effects when, as in TARE treatments, a VOI segmentation is carried out. The recovery of partial volume effect can be more effectively applied when active volumes can be associated with morphologic volumes in high-resolution morphologic imaging (CT), as in the case of whole Liver. On the contrary, when an active volume is segmented from

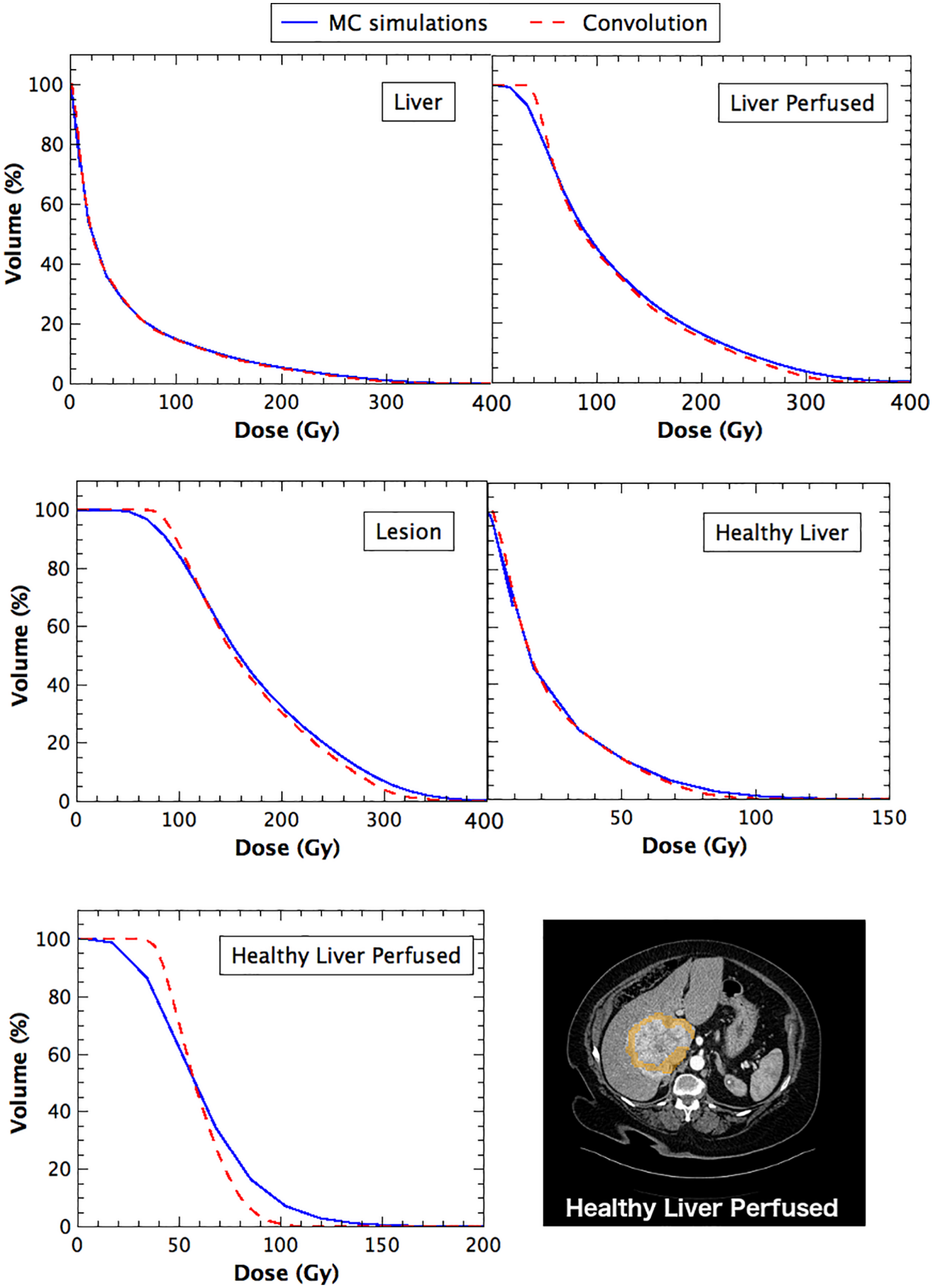

Fig. 3. DVHs in the five structures of patient #6: Liver, Liver Perfused, Lesion, Healthy Liver, and Healthy Liver Perfused. Last panel shows the shape of Healthy Liver Perfused, as resulting from a logical subtraction between Liver Perfused and Lesion.

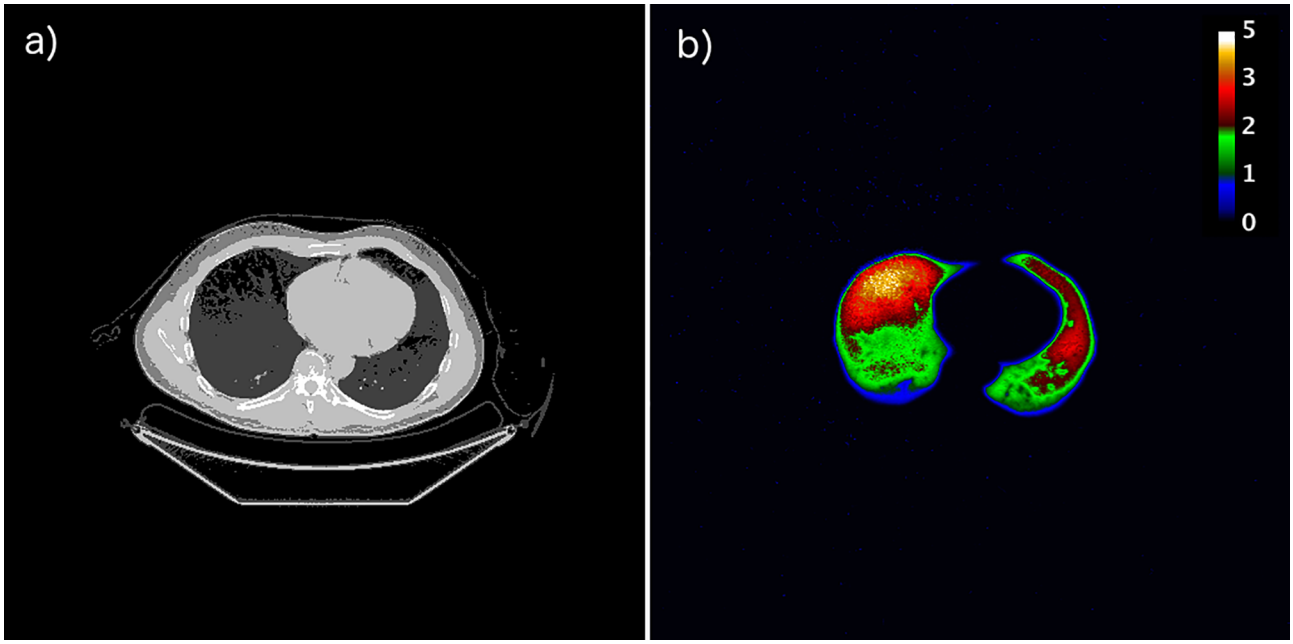

Fig. 4. (a) A CT slice of the segmented phantom (patient #5) showing the lungs above liver and (b) the corresponding absorbed dose map in Gy.

Table 3
Average radiation absorbed doses to the lungs of patient #5.

	LEFT	RIGHT
Lung shunt (%)	1.00	1.00
Dose from pulmonary shunt (Gy)	2.07	2.05
Dose from Liver Exposure (Gy)	0.0017	0.0902
D_{tot} (Gy)	2.07	2.14

SPECT imaging, as in the case of Liver Perfused, the diffuse gradient of uptake is further smoothed by the low resolution of scanner. For these reasons, some Authors have questioned about the opportunity to apply a convolution calculation approach to derive 3D dosimetry, when low-resolution 3D TIA maps are to be used as input, supporting the thesis of a 3D dosimetry based on Local Energy Deposition (LED) of electrons in source voxels [24]. In this framework, MC approaches like ours, even if biased by the same limitation of low-resolution 3D source distribution, have – with respect to convolution methods – the advantage of correctly propagating long-range radiations (gamma-rays) and of accurately accounting for differences in tissue densities and compositions.

Finally, one has to bear in mind that a pre-therapeutic dosimetry based on a diagnostic angio-scintigraphy with ^{99m}Tc-MAA will differ from the actual dose distribution delivered, in a separate and subsequent interventional procedure, by ^{90}Y-microspheres [40].

5. Conclusions

The Monte Carlo simulation of radiation transport and interaction is the most accurate method for evaluating the radiation absorbed dose distribution in internal radiotherapies with radionuclides, and can give a valuable contribution in the direction of providing three-dimensional dosimetry in nuclear medicine treatments. We developed a procedure exploiting GAMOS and tested our method on clinical cases of TARE of HCC, comparing our results with those obtained using other calculation methods.

3D absorbed dose maps, absorbed dose profiles and absorbed Dose Volume Histograms were produced, highlighting the importance of such data, in particular at the interface between tissues of different density and composition.

For most patients, we found a good agreement between MIRD approach, convolution method (as implemented in the STRATOS software) and MC simulations; some discrepancy was observed for VOIs for which the contribution from gamma-rays has to be carefully modelled and taken into account.

MC simulation allowed us to estimate mean absorbed dose to lungs, which exhibits maximum values in proximity of the liver-lung interface.

We can conclude that 3D dosimetry for TARE treatments of HCC can be satisfactorily carried out with convolution methods as long as VOIs of regular shape are considered. MC simulations are more appropriate for VOIs where the contribution from gamma-rays has to be carefully taken into account. Nevertheless, the absorbed dose distribution in presence of relevant tissue inhomogeneities can be assessed accurately by means of MC simulations only.

Appendix A. Supplementary data

Supplementary data to this article can be found online at https://doi.org/10.1016/j.ejmp.2019.07.024.

References

[1] Stokke C, Gabiña PM, Solný P, Cicone F, Sandström M, Gleisner KS, et al. Dosimetry-based treatment planning for molecular radiotherapy: a summary of the 2017 report from the Internal Dosimetry Task Force. EJNMMI Phys 2017;4:27. https://doi.org/10.1186/s40658-017-0194-3.
[2] Li T, Ao ECI, Lambert B, Brans B, Vandenberghe S, Mok GSP. Quantitative imaging for targeted radionuclide therapy dosimetry – technical review. Theranostics 2017;7:4551–65. https://doi.org/10.7150/thno.19782.
[3] Strigari L, Konijnenberg M, Chiesa C, Bardies M, Du Y, Gleisner KS, et al. The evidence base for the use of internal dosimetry in the clinical practice of molecular radiotherapy. Eur J Nucl Med Mol Imaging 2014;41:1976–88. https://doi.org/10.1007/s00259-014-2824-5.
[4] Pacilio M, Amato E, Lanconelli N, Basile C, Torres LA, Botta F, et al. Differences in 3D dose distributions due to calculation method of voxel S-values and the influence of image blurring in SPECT. Phys Med Biol 2015;60:1945–64. https://doi.org/10.1088/0031-9155/60/5/1945.
[5] Amato E, Cicone F, Auditore L, Baldari S, Prior JO, Gnesin S. A Monte Carlo model for the internal dosimetry of choroid plexuses in nuclear medicine procedures. Phys Medica 2018;49:52–7. https://doi.org/10.1016/j.ejmp.2018.05.005.
[6] Amato E, Minutoli F, Pacilio M, Campennì A, Baldari S. An analytical method for computing voxel S values for electrons and photons. Med Phys 2012;39:6808–17. https://doi.org/10.1118/1.4757912.
[7] Giap HB, Macey DJ, Bayouth JE, Boyer AL. Validation of a dose-point kernel convolution technique for internal dosimetry. Phys Med Biol 1995;40:365–81. https://doi.org/10.1088/0031-9155/40/3/003.
[8] Dieudonné A, Garin E, Laffont S, Rolland Y, Lebtahi R, Leguludec D, et al. Clinical

feasibility of fast 3-dimensional dosimetry of the liver for treatment planning of hepatocellular carcinoma with 90Y-microspheres. J Nucl Med 2011;52:1930–7. https://doi.org/10.2967/jnumed.111.095232.
[9] Kafrouni M, Allimant C, Fourcade M, Vauclin S, Delicque J, Ilonca A-D, et al. Retrospective voxel-based dosimetry for assessing the ability of the body-surface-area model to predict delivered dose and radioembolization outcome. J Nucl Med 2018;59:1289–95. https://doi.org/10.2967/jnumed.117.202937.
[10] Amato E, Italiano A, Baldari S. Monte Carlo study of voxel S factor dependence on tissue density and atomic composition. Nucl Instruments Methods Phys Res Sect A 2013;729:870–6. https://doi.org/10.1016/j.nima.2013.08.059.
[11] Khazaee Moghadam M, Kamali Asl A, Geramifar P, Zaidi H. Evaluating the application of tissue-specific dose kernels instead of water dose kernels in internal dosimetry: a Monte Carlo study. Cancer Biother Radiopharm 2016;31:367–79. https://doi.org/10.1089/cbr.2016.2117.
[12] Sanchez-Garcia M, Gardin I, Lebtahi R, Dieudonné A. Implementation and validation of collapsed cone superposition for radiopharmaceutical dosimetry of photon emitters. Phys Med Biol 2015;60:7861–76. https://doi.org/10.1088/0031-9155/60/20/7861.
[13] Bolch WE, Bouchet LG, Robertson JS, Wessels BW, Siegel JA, Howell RW, et al. MIRD pamphlet No. 17: the dosimetry of nonuniform activity distributions–radionuclide S values at the voxel level. Medical Internal Radiation Dose Committee. J Nucl Med 1999;40(1):11S–36S.
[14] Furhang EE, Chui CS, Kolbert KS, Larson SM, Sgouros G. Implementation of a Monte Carlo dosimetry method for patient-specific internal emitter therapy. Med Phys 1997;24:1163–72. https://doi.org/10.1118/1.598018.
[15] Yoriyaz H, Stabin MG, dos Santos A. Monte Carlo MCNP-4B-based absorbed dose distribution estimates for patient-specific dosimetry. J Nucl Med 2001;42(4):662–9.
[16] Ljungberg M, Sjögreen K, Liu X, Frey E, Dewaraja Y, Strand S-E. A 3-dimensional absorbed dose calculation method based on quantitative SPECT for radionuclide therapy: evaluation for 131 i using Monte Carlo simulation. J Nucl Med 2002;43(8):1101–9http://jnm.snmjournals.org/content/43/8/1101.abstract.
[17] Marcatili S, Pettinato C, Daniels S, Lewis G, Edwards P, Fanti S, et al. Development and validation of RAYDOSE: a Geant4-based application for molecular radiotherapy. Phys Med Biol 2013;58:2491–508. https://doi.org/10.1088/0031-9155/58/8/2491.
[18] Grimes J, Uribe C, Celler A. JADA: A graphical user interface for comprehensive internal dose assessment in nuclear medicine. Med Phys 2013;40:072501https://doi.org/10.1118/1.4810963.
[19] Kost SD, Dewaraja YK, Abramson RG, Stabin MG. VIDA: a voxel-based dosimetry method for targeted radionuclide therapy using Geant4. Cancer Biother Radiopharm 2015;30:16–26. https://doi.org/10.1089/cbr.2014.1713.
[20] Besemer AE, Yang YM, Grudzinski JJ, Hall LT, Bednarz BP. Development and validation of RAPID: a patient-specific Monte Carlo three-dimensional internal dosimetry platform. Cancer Biother Radiopharm 2018;33:155–65. https://doi.org/10.1089/cbr.2018.2451.
[21] Petitguillaume A, Bernardini M, Hadid L, De Labriolle-Vaylet C, Franck D, Desbrée A. Three-dimensional personalized Monte Carlo dosimetry in 90Y resin microspheres therapy of hepatic metastases: nontumoral liver and lungs radiation protection considerations and treatment planning optimization. J Nucl Med 2014;55:405–13. https://doi.org/10.2967/jnumed.113.120444.
[22] Hashikin NAA, Yeong CH, Guatelli S, Abdullah BJJ, Ng KH, Malaroda A, et al. Systematic investigation on the validity of partition model dosimetry for 90Y radioembolization using Monte Carlo simulation. Phys Med Biol 2017;62:7342–56. https://doi.org/10.1088/1361-6560/aa7e5b.
[23] Ho S, Lau WY, Lung TWT, Chan M, Ngar YK, Johnson PJ, et al. Partition model for estimating radiation doses from Yttrium-90 microspheres in treating hepatic tumors. Eur J Nucl Med 1996;23(8):947–52. https://doi.org/10.1007/BF01084369.
[24] Chiesa C, Mira M, Maccauro M, Spreafico C, Romito R, Morosi C, et al. Radioembolization of hepatocarcinoma with 90Y glass microspheres: development of an individualized treatment planning strategy based on dosimetry and radiobiology. Eur J Nucl Med Mol Imaging 2015;42:1718–38. https://doi.org/10.1007/s00259-015-3068-8.
[25] Gulec SA, Mesoloras G, Stabin M. Dosimetric techniques in ^{90}Y-microsphere therapy of liver cancer: the MIRD equations for dose calculations. J Nucl Med 2006;47:1209–11.
[26] Arce P, Rato P, Cañadas M, Gamos Lagares JI. A GEANT4-based easy and flexible framework for nuclear medicine applications. IEEE Nucl Sci Symp Conf Rec 2008:3162–8. https://doi.org/10.1109/NSSMIC.2008.4775023.
[27] Agostinelli S, et al. Geant4 – a simulation toolkit. Nucl Instrum Methods A 2003;506:250–303. https://doi.org/10.1016/S0168-9002(03)01368-8.
[28] Allison J, et al. Geant4 developments and applications. IEEE Trans Nucl Sci 2006;53:270–8.
[29] Allison J, et al. Recent developments in Geant4. Nucl Instrum Meth A 2016;835:186–225.
[30] Paulus T, Fischer A, van Loon P, Schweizer B, Gegenmantel E, Bippus R. IMALYTICS: the philips translational and research workstation. Medicamundi 2010;54(2):78–81.
[31] Bolch WE, Eckerman KF, Sgouros G, Thomas SR, Brill AB, Fisher DR, et al. MIRD pamphlet No. 21: a generalized schema for radiopharmaceutical dosimetry-standardization of nomenclature. J Nucl Med 2009;50:477–84. https://doi.org/10.2967/jnumed.108.056036.
[32] Geant4 Reference Physics Manual, version geant4 10.3, n.d. http://geant4.cern.ch.
[33] ENSDF, Evaluated Nuclear Structure Data File, Maint. by Natl. Nucl. Data Cent. Brookhaven Natl. Lab. (n.d.). http://www.nndc.bnl.gov/ensdf/.
[34] Tuli J, Evaluated nuclear structure data file, BNL-NCS-51655-Rev87; 1987.
[35] Berenato S, Amato E, Fischer A, Baldari S. Influence of voxel S factors on three-dimensional internal dosimetry calculations. Phys Medica 2016;32(10):1259–62.
[36] Bouchet LG, Bolch WE, Weber DA, Atkins HL, Poston Sr. JW. MIRD Pamphlet No. 15: radionuclide S values in a revised dosimetric model of the adult head and brain. Medical Internal Radiation Dose. J Nucl Med 1999;40:62S–101S.
[37] Chiavassa S, Aubineau-Lanièce I, Bitar A, et al. Validation of a personalized dosimetric evaluation tool (Oedipe) for targeted radiotherapy based on the Monte Carlo MCNPX code. Phys Med Biol 2006;51:601–16.
[38] Pelowitz DB. MCNPX User's manual version 2.6.0. Technical report LA-CP-05-0369. Los Alamos, NM: Los: Alamos National Laboratory; 2008.
[39] Braad PEN, Andersen T, Hansen SB, Høilund-Carlsen PF. Strategies for CT tissue segmentation for Monte Carlo calculations in nuclear medicine dosimetry: strategies for CT tissue segmentation for Monte Carlo calculations. Med Phys 2016;43(12):6507–16.
[40] Rhee S, Kim S, Cho J, Park J, Eo JS, Park S, et al. Semi-quantitative analysis of post-transarterial radioembolization ^{90}Y microsphere positron emission tomography combined with computed tomography (PET/CT) images in advanced liver malignancy: comparison with ^{99m}Tc macroaggregated albumin (MAA) single photon emission computed tomography (SPECT). Nucl Med Mol Imaging 2016;50(1):63–9.